Oblique Wave Scattering by a Floating Elastic Plate over a Porous Bed in Single and Two-layer Fluid Systems

H. Behera[a], Chiu-On Ng[b,*], T. Sahoo[c]

[a]*Department of Mathematics, SRM University, Kattankulathur, Chennai, India*
[b]*Department of Mechanical Engineering, The University of Hong Kong, Pokfulam Road, Hong Kong, China*
[c]*Department of Ocean Engineering and Naval Architecture, Indian Institute of Technology Kharagpur, India*

Abstract

An analytical study is presented in this paper for oblique wave scattering by a floating elastic plate in a one or two-layer body of water over a porous seabed of infinite depth. The solution procedure adopted, under the assumption of small-amplitude surface waves and structural response, is the eigenfunction expansion method. The study aims to look into the interaction between oblique waves and a floating elastic plate that serves as an effective breakwater. Effects of three types of edge conditions, viz. (i) free edge, (ii) simple-supported edge, and (iii) clamped edge are analyzed. Numerical results for the reflection and transmission coefficients are computed and examined for various values of the wave, porous bed and structural parameters. Results for wave interaction with an elastic plate over a non-porous bed are obtained as special cases and compared with results available in the literature. The study reveals that for various combinations of wave and structural parameters, zero reflection and full transmission may occur in case of rigid bottom and real porous-effect parameter of the porous bed. However, for complex porous-effect parameter, zero reflection and full transmission do not occur. Moreover, due to the energy dissipation by porous bed, wave transmission decreases significantly with increase in length of the floating plate in case of complex porous-effect parameter. The results will be useful in the design of breakwaters for the protection of harbors, inlets and beaches against attacks from surface waves.

Keywords: Oblique waves; porous seabed; floating elastic plate; two-layer fluid.

1. Introduction

Over the past few decades, marine floating structures have been extensively investigated, by researchers as well as practicing engineers, for a wide range of applications in ocean and coastal engineering. The main advantage of floating structures is that they allow free passage of currents, thereby avoiding undesirable problems such as sediment deposition near the structures. In particular, there has been an increasing interest in the use of flexible floating structures as breakwaters, since flexible structures may enhance wave attenuation through wave–structure interaction, and most importantly,

*Corresponding Author
Email addresses: hkb.math@gmail.com (H. Behera), cong@hku.hk (Chiu-On Ng), tsahoo1967@gmail.com (T. Sahoo)

these structures are light in weight, cost-effective, reusable and environmental friendly. A variety of mathematical techniques have been developed for wave interaction with floating or submerged structures. Various aspects of wave interaction with very large floating structures have been examined by, among many others, Fox and Squire (1994), Meylan and Squire (1996), and Chen et al. (2006). Using Fourier analysis and a newly developed inner product, Sahoo et al. (2001) studied the scattering of surface waves by a floating semi-infinite elastic plate in a two-dimensional water domain of finite depth. Meanwhile, Teng et al. (2001) applied a modified eigenfunction method to wave interaction with a semi-infinite elastic plate. Sturova (2009) developed the time-domain mode-expansion method for hydroelastic analysis of the heterogeneous plate floating on shallow water of variable depth. Oblique scattering of waves by a moored finite floating elastic plate with changes in bottom topography was recently examined by Karmakar and Soares (2012). Papathanasiou et al. (2015) developed model based on finite element method for two-dimensional problems concerning the response of large floating elastic bodies, in an inhomogeneous shallow water environment, characterized by variable bathymetry and thickness distribution. An experimental validation of theoretical models of regular-water-wave transmission through arrays of floating disks is investigated by Bennetts and Williams (2015). Moreover, the presence of thermal strain, surface friction due to wind and water flow beneath the ice are the natural sources of compressive stress on a floating ice sheet. In case of a large compressive force, buckling phenomena occurs and details of this phenomena has been studied by Mohanty et al. (2014) in case of flexural-gravity wave motion over rigid bed. Apart from wave interaction with floating structures, there has been a parallel interest in the problems of wave interaction with submerged structures. Hassan et al. (2009) analyzed the surface wave interaction with submerged flexible plates of finite and semi-infinite length in two- and three-dimensional fluid domains. Williams and Meylan (2012) presented an analytical study on the surface wave interaction with a semi-infinite submerged elastic plate using the Wiener-Hopf technique.

There is a sizeable body of literature on the study of full/partial (i.e., fully or partially extended across the water column) porous breakwater of finite width, using the model of Sollitt and Cross (1972). Oblique wave transmission by fully extended porous structures was studied by Dalrymple et al. (1991), followed by Losada et al. (1996) who studied wave interaction with submerged porous structures. A thorough review on wave interaction with various perforated breakwaters can be found in Huang et al. (2011). To avoid the complex dispersion relation within the porous medium, Liu and Li (2013) developed an alternative analytic solution method for wave past a porous structure. Koley et al. (2015) used a boundary element method to study wave interaction with bottom-standing submerged structures that have a perforated outer-layer and are placed on a sloping bed.

In coastal waters, density stratifications often happen as a result of solar heating or the meeting of fresh water with salty water in estuarine regions. Recently, there has been a growing interest in studying wave–structure interaction in a two-layer fluid system by considering an upper lighter fluid of density ρ_1 overlying a heavier fluid of density ρ_2. Various aspects of wave motion in a two-layer fluid have been studied by Linton and McIver (1995), Sherief et al. (2004), Kashiwagi et al. (2006), and the references cited therein. Bhattacharjee and Sahoo (2008) looked into problems of flexural gravity waves in a two-layer fluid. Xu and Lu (2010) and Lin and Lu (2013) also presented analytical models

for interaction between waves and a floating elastic plate in a two-layer fluid. Recently, oblique wave interaction with flexible and porous barriers in a two-layer fluid was examined by Behera et al. (2013).

Unlike wave propagation over impermeable rigid bed, in the case of water wave propagation over a permeable seabed various dissipation mechanisms associated with the porous medium contribute to wave damping and thus transforms the wave characteristics. An enhanced coupled-mode system is developed by Belibassakis (2012) for modeling wave-induced pressure and groundwater flow in variable bathymetry coastal regions, in the layer under the permeable seabed. On the other hand, to study wave motion over a porous seabed, a special type of porous bed condition was used by Martha et al. (2007) and Maiti and Mandal (2014), in which the fluid flow within the porous bed is not taken into consideration and the porosity parameter is similar to the porous-effect parameter introduced by Yu and Chwang (1994) with the resistance effect being predominant. In this model, the rigid bed condition is replaced by a boundary condition which is assumed to be a porous bed. The bed depth is assumed to be infinitely extended. The fluid motions are such that the resulting boundary condition on the sea-bed used holds good agreement and depends on a known parameter G which has a dimension of $(length)^{-1}$, called the porous-effect parameter. This assumption ensures the existence of plane wave solution that will decay otherwise at the far field in the open-water region. To the authors' knowledge, there exists no study in the literature that considers oblique wave scattering by a floating elastic plate in a single or two-layer fluid over such a seabed.

The present work aims to look into the problem of oblique wave scattering by a floating flexible plate over a porous bed as discussed above in both the cases of single and two-layer fluids with the assumption that there exist an interface in case of the two-layer fluid. It may be noted that the physical problems for single and two-layer are different from practical point of view. For example, in case of a homogeneous fluid, a single plane progressive wave will propagate due to the presence of the free surface. On the other hand, in two-layer fluid, plane progressive waves in surface and internal modes will propagate due to the presence of the free surface and interface. As a result, incident, reflected and transmitted wave characteristics in surface and internal modes are discussed in case of two-layer fluids which is not the case for homogeneous single-layer fluid. The mathematical problems are formulated under the assumption of small amplitude water wave theory and structural response. It is also assumed that the flexible plate is under the action of a uniform compressive force. Effect of three different types of edge conditions, namely, clamped edge, simply-supported edge, and free edge are analyzed in the present study. The roots of the dispersion relation in the open-water and plate-covered regions over a porous bed are analyzed using contour plots. In case of two-layer fluid, due to the presence of the interface, there exist waves modes in the surface and internal modes in both the cases of the open water region and plate covered region. Thus, in the case of two-layer fluid, the reflection and transmission coefficients exist in surface and internal modes. Moreover, in the present study, the porous-effect parameter which signifies the bed porosity is assumed to be a complex number to account for the both the inertia and resistance effects. Various numerical results for the reflection and transmission coefficients are computed and analyzed to study the effects compressive force, length of the plate, porous-effect parameter of the porous bed, oblique angle of incidence, structural rigidity of the plate, position of the interface and density ratio. The computed results are compared with those

available in the literature for the special case of wave scattering by a floating elastic plate over a non-porous/porous bed in a single/two-layer fluid system.

2. Wave scattering by a floating elastic plate in a single-layer fluid system

In this subsection, wave scattering by a floating elastic plate over a porous bed is studied for a homogeneous fluid.

2.1. Mathematical formulation

Three-dimensional Cartesian coordinates are chosen wherein the z-axis is taken vertically downward positive into the fluid region with ($z = 0$) being the undisturbed free surface, and the x-y plane is considered as a horizontal plane. It is assumed that a thin elastic plate having length b and uniform thickness d floats on the mean free surface $z = 0$ of a fluid medium of uniform density ρ and water of finite depth H. In the present study, for dealing with more realistic physical situation in which both the resistance and inertia effects will contribute for energy dissipation by the seabed, the porous-effect parameter is assumed to be complex in nature unlike in the work of Martha et al. (2007) and Maiti and Mandal (2014) in which the porous-effect parameter was assumed to be a real number to ensure progressive wave at the far field. Moreover, in the present study, the fluid motion inside the porous bed is not considered. Since water depth is finite, only boundary condition at interface between fluid and porous bed is used to handle the physical problem under the assumption that the porous seabed is infinitely extended in the horizontal direction. The whole fluid domain is divided into three subdomains as shown in Fig. 1, namely, the open-water region ($x < 0$) as region 1, the region below the flexible plate ($0 < x < b$) as region 2, and the open-water region ($x > b$) as region 3. The fluid is assumed to be inviscid, incompressible, and the fluid motion is considered irrotational and simple harmonic in time with an angular frequency ω, which ensures the existence of velocity potentials $\Phi_j(x, y, z, t)$ for $j = 1, 2, 3$ in the three regions.

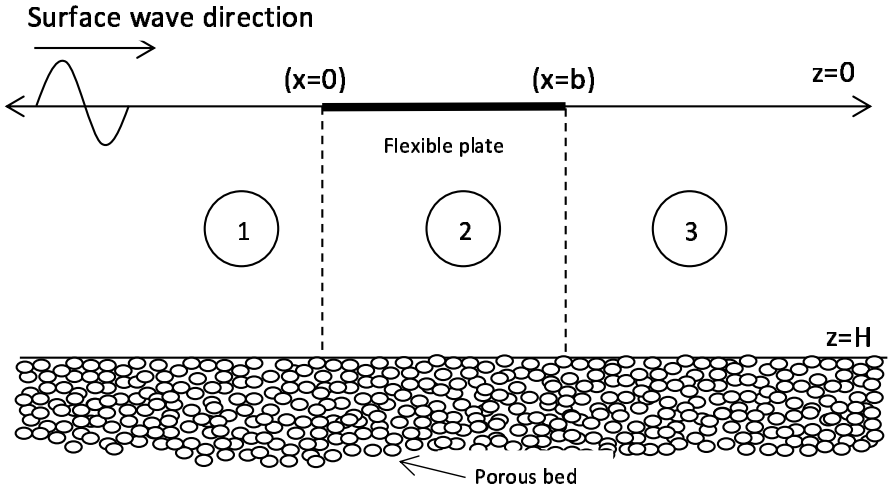

Figure 1 Schematic diagram of wave scattering by floating elastic plate over a porous bed in single-layer fluid.

The velocity potentials Φ_j for $j = 1, 2, 3$ satisfy the three-dimensional Laplace equation given by

$$\left(\frac{\partial^2}{\partial x^2} + \frac{\partial^2}{\partial y^2} + \frac{\partial^2}{\partial z^2}\right)\Phi_j = 0. \tag{1}$$

The boundary condition on the permeable bed is given by, as in Martha et al. (2007) and Maiti and Mandal (2014),

$$\frac{\partial \Phi_j}{\partial z} - G\Phi_j = 0 \quad \text{on } z = H, \quad \text{for} \quad j = 1, 2, 3, \tag{2}$$

where G is the porous-effect parameter characterizing the bed permeability having dimension of length. In general, the porous-effect parameter is a complex number to account for both the resistance and inertia effect as in Yu and Chwang (1994). It may be noted that to ensure propagation of progressive wave at the far field in the open water region, G was assumed to be a real number (see Maiti and Mandal (2014). Assuming that there is no gap between air and water as well as the fluid and the floating elastic plate, the linearized kinematic condition on the mean free surface yields

$$\frac{\partial \Phi_j}{\partial z} = \frac{\partial \eta_j}{\partial t} \quad \text{on} \quad z = 0 \quad \text{for } j = 1, 2, 3, \tag{3}$$

where η_1 and η_3 are the free surface elevations in the open-water regions 1 and 3, respectively, and η_2 is the deflection of the floating plate. The linearized dynamic condition on the mean free surface in regions 1 and 3 yield

$$\frac{\partial \Phi_j}{\partial t} = g\eta_j \quad \text{on} \quad z = 0 \quad \text{for } j = 1, 3, \tag{4}$$

where g is the acceleration due to gravity. Eliminating η_j for $j = 1, 3$ from the kinematic and dynamic conditions given by Eqs. (3) and (4), the linearized free-surface boundary conditions in the open-water regions 1 and 3 are obtained as follows:

$$\frac{\partial^2 \Phi_j}{\partial t^2} = g\frac{\partial \Phi_j}{\partial z} \quad \text{on } z = 0 \text{ for } j = 1, 3, \tag{5}$$

Moreover, from Bernoulli's equation, the linearized pressure $P_h(x, y, z, t)$ acting on the floating plate, as in Mohanty et al. (2014), is obtained as

$$P_h = -\rho\frac{\partial \Phi_2}{\partial t} + \rho g\eta_2 \text{ on } z = 0. \tag{6}$$

In the presence of a uniform compressive force N along the x-y plane, the thin plate equation yields

$$\left(EI\nabla_{xy}^4 + N\nabla_{xy}^2 + \rho_e d\frac{\partial^2}{\partial t^2}\right)\eta_2 = -P_h, \tag{7}$$

where E and ρ_e are Young's modulus and density of the elastic plate, respectively, with $I = d^3/[12(1-\nu^2)]$ and ν being the Poisson ratio of the elastic plate. Using Eqs. (3), (6) and (7), the linearized plate-covered boundary condition is obtained as

$$\left(EI\nabla_{xy}^4 + N\nabla_{xy}^2 + \rho_e d\frac{\partial^2}{\partial t^2} + \rho g\right)\frac{\partial \Phi_2}{\partial z} = \rho\frac{\partial^2 \Phi_2}{\partial t^2} \quad \text{on} \quad z = 0. \tag{8}$$

Moreover, assuming that the incident wave is propagating at an angle θ with respect to the x-axis, the velocity potentials and free surface elevations in each region are of the form $\Phi_j(x,y,z,t) = \mathrm{Re}\{\phi_j(x,z)\mathrm{e}^{\mathrm{i}(\mu_y y-\omega t)}\}$ and $\eta_j(x,y,t) = \mathrm{Re}\{\bar{\eta}(x)e^{\mathrm{i}(\mu_y y-\omega t)}\}$, respectively, for $j = 1,2,3$, where $\mu_y = k_0 \sin\theta$ with k_0 being the wave number of the plane gravity wave. Thus, the spatial velocity potential $\phi_j(x,z)$ for $j = 1,2,3$ will satisfy the Helmholtz equation given by

$$\left(\frac{\partial^2}{\partial x^2} + \frac{\partial^2}{\partial z^2} - \mu_y^2\right)\phi_j = 0, \quad \text{for} \quad j = 1,2,3, \tag{9}$$

along with the boundary conditions as in Eqs. (2)–(5). Further, using Eq. (1), the dynamic boundary condition as in Eq. (8) can be rewritten as (following Mohapatra et al. (2013))

$$\left(D\frac{\partial^4}{\partial z^4} - Q\frac{\partial^2}{\partial z^2} - MK + 1\right)\frac{\partial \phi_2}{\partial z} + K\phi_2 = 0, \tag{10}$$

where $D = EI/\rho g$, $Q = N/\rho g$, $K = \omega^2/g$ and $M = \rho_e d/\rho$. Further, the continuity of pressure and velocity near the fluid structure interfaces at $x = 0$ and $x = b$ yield

$$\phi_j(0,z) = \phi_2(0,z), \quad \frac{\partial \phi_j(0,z)}{\partial x} = \frac{\partial \phi_2(0,z)}{\partial x}, \tag{11}$$

where $j = 1$ at $x = 0$ and $j = 3$ at $x = b$. It is assumed that the edges of the floating plate are either free, simply-supported, or clamped. In the case of free edges, the bending moment and shear force are zero on the edges and the conditions are given by

$$EI\left(\frac{\partial^2}{\partial x^2} - \nu\mu_y^2\right)\frac{\partial \phi_2}{\partial z} = 0, \quad \left[EI\left\{\frac{\partial^2}{\partial x^2} - (2-\nu)\mu_y^2\right\}\frac{\partial}{\partial x} + Q\frac{\partial}{\partial x}\right]\frac{\partial \phi_2}{\partial z} = 0 \quad \text{at} \quad (0,0) \quad \text{and} \quad (b,0). \tag{12}$$

In the case of simply-supported edges, the deflection and bending moment of the plate are zero and the conditions are given by

$$\frac{\partial \phi_2}{\partial z} = 0, \quad EI\left(\frac{\partial^2}{\partial x^2} - \nu\mu_y^2\right)\frac{\partial \phi_2}{\partial z} = 0 \quad \text{at} \quad (0,0) \quad \text{and} \quad (b,0), \tag{13}$$

while the plate deflection and slope of the plate deflection are zero in the case of clamped edges, and the conditions are given by

$$\frac{\partial \phi_2}{\partial z} = 0, \quad \frac{\partial^2 \phi_2}{\partial x \partial z} = 0 \quad \text{at} \quad (0,0) \quad \text{and} \quad (b,0). \tag{14}$$

Finally, the radiation condition for oblique wave scattering by a floating elastic plate over a porous bed yields

$$\phi_j(x,z) = \begin{cases} \left(I_0 e^{iq_0 x} + R_0 e^{-iq_0 x}\right) f_0(k_0,z), & j = 1, x \to -\infty, \\ T_0 e^{iq_0 x} f_0(k_0,z), & j = 3, x \to \infty, \end{cases} \tag{15}$$

where I_0 is the known constant associated with the amplitude of the incident wave, R_0 and T_0 are the unknown constants associated with the reflected and transmitted wave amplitudes respectively, with

$q_0 = \sqrt{k_0^2 - \mu_y^2}$ and k_0 being the most predominant progressive wave number which is a complex number in general. However, in case of real G, k_0 becomes a real positive number. Details about the roots of the dispersion relation will be discussed in the subsequent Section.

$$k_0(k_0 \tanh k_0 H - G) = K(k_0 - G \tanh k_0 H). \tag{16}$$

Further, in Eq. (15), $f_0(k_0, z)$ is the eigenfunction associated with k_0 and is given by

$$f_0(k_0, z) = \left(\frac{\mathrm{i}g}{\omega}\right) \frac{k_0 \cosh k_0(H - z) - G \sinh k_0(H - z)}{\cosh k_0 H - G \sinh k_0 H}. \tag{17}$$

2.2. Method of solution

The spatial velocity potentials in regions 1, 2 and 3 satisfying the governing equation (9) along with the boundary conditions prescribed in Eqs. (2), (5) and (15), are written as

$$\phi_j(x, z) = \begin{cases} I_0 \mathrm{e}^{\mathrm{i}q_0 x} f_0(k_0, z) + \displaystyle\sum_{n=0}^{\infty} R_n \mathrm{e}^{-\mathrm{i}q_n x} f_n(k_n, z), & \text{for} \quad x < 0, j = 1, \\ \displaystyle\sum_{n=0}^{\infty} \left\{A_n \mathrm{e}^{\mathrm{i}Q_n x} + B_n \mathrm{e}^{-\mathrm{i}Q_n (x-b)}\right\} g_n(p_n, z), & \text{for} \quad 0 < x < b, j = 2, \\ \displaystyle\sum_{n=0}^{\infty} T_n \mathrm{e}^{\mathrm{i}q_n (x-b)} f_n(k_n, z), & \text{for} \quad x > b, j = 3, \end{cases} \tag{18}$$

where R_n, A_n, B_n and T_n for $n = 0, 1, 2, \cdots$ are unknown expansion coefficients to be determined with $q_n = \sqrt{k_n^2 - \mu_y^2}$ and $Q_n = \sqrt{p_n^2 - \mu_y^2}$, and the eigenfunctions $f_n(k_n, z)$ and $g_n(p_n, z)$ are given by

$$f_n(k_n, z) = \left(\frac{\mathrm{i}g}{\omega}\right) \frac{k_n \cosh k_n(H - z) - G \sinh k_n(H - z)}{\cosh k_n H - G \sinh k_n H}, \tag{19}$$

$$g_n(p_n, z) = \left(\frac{\mathrm{i}g}{\omega}\right) \frac{p_n \cosh p_n(H - z) - G \sinh p_n(H - z)}{\cosh p_n H - G \sinh p_n H}. \tag{20}$$

In the open-water regions 1 and 3, the eigenvalues k_n satisfy the dispersion relation

$$k_n(k_n \tanh k_n H - G) = K(k_n - G \tanh k_n H). \tag{21}$$

On the other hand, in the plate-covered region 2, the eigenvalues p_n satisfy the dispersion relation

$$\left(D p_n^4 - Q p_n^2 - MK + 1\right)\left(p_n^2 \tanh p_n H - p_n G\right) = K(p_n - G \tanh p_n H). \tag{22}$$

The eigenfunctions in the open-water regions $f_n(k_n, z)$ are orthonormal, i.e.,

$$\int_0^H f_n(k_n, z) f_m(k_m, z) dz = \delta_{nm}, \tag{23}$$

where δ_{nm} is the Kronecker delta. However, the vertical eigenfunctions in the plate-covered region are not orthogonal as has been discussed by Sahoo et al. (2001). In the present study, orthogonality of the eigenfunction in the open-water regions are used to solve the boundary-value problem.

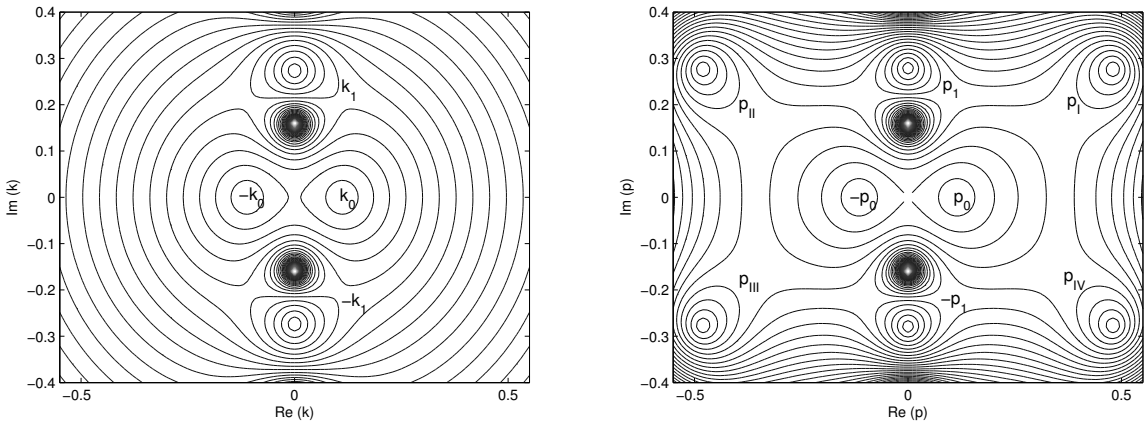

(a) (b)

Figure 2 Contour plots of roots of the dispersion relation for (a) open-water region and (b) plate-covered region in single-layer fluid over porous bed with $H = 10$m, $T = 8$sec., $g = 9.81$ m/sec^2, $\nu = 0.3$, $GH = 0.5$, $E = 1$ GPa, $d = 0.1$ and $N = \sqrt{EI\rho g}$.

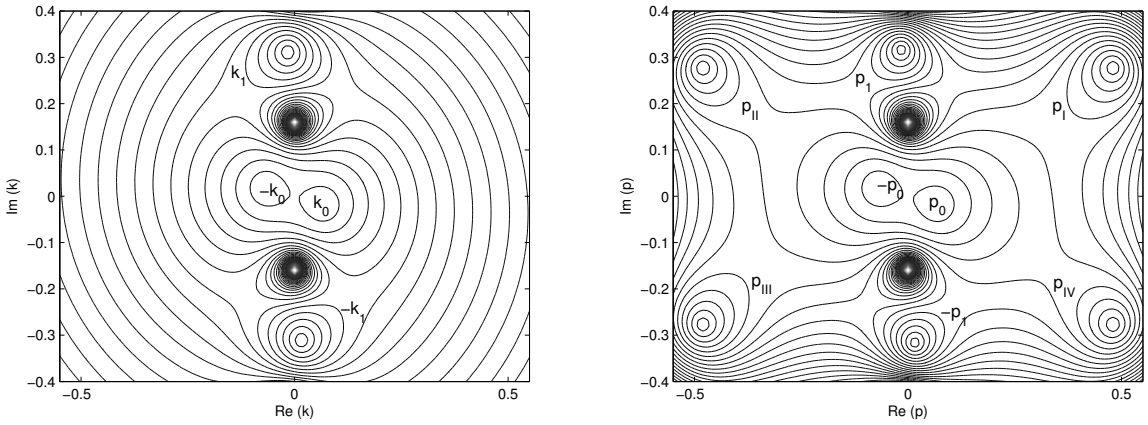

(a) (b)

Figure 3 Contour plots of roots of the dispersion relation for (a) open-water region and (b) plate-covered region in single-layer fluid over porous bed with $H = 10$m, $T = 8$sec., $g = 9.81$ m/sec^2, $\nu = 0.3$, $GH = 0.5 + 0.5i$, $E = 1$ GPa, $d = 0.1$ and $N = \sqrt{EI\rho g}$.

It may be noted that for $G = 0$ and $Q = 0$, the dispersion relation in Eqs. (21) and (22) reduce to the dispersion relations for the open-water and plate-covered regions, respectively, over a non-porous bed as in Maiti and Mandal (2014). In the present work, the nature of the roots of the dispersion relation in the open-water and plate-covered regions as given in Eqs. (21) and (22) are analyzed in Figs. 2(a, b) using contour plots as has been performed by Fox and Squire (1990). For determining the roots of the dispersion equations in the open water and plate-covered regions, Newton-Raphson method is used. Initial guess in the Newton-Raphson method for each root is obtained using contour

plot. Unlike gravity waves over a non-porous bed, Fig. 2(a) reveals that the dispersion relation in Eq. (21) has two real roots $\pm k_0$. Further, it has infinite many imaginary roots of opposite signs $\pm k_n$, $n = 1, 2, 3, \cdots$, which imply the existence of evanescent modes of which only the first few roots are shown here. On the other hand, unlike flexural gravity wave motion over a non-porous bed, Fig. 2(b) shows that the dispersion relation given in Eq. (22) has two real roots $\pm p_0$, four complex roots p_I, p_{II}, p_{III} and p_{IV}, with $p_I = \bar{p}_{IV}$ and $p_{II} = \bar{p}_{III}$, which are non-propagating in nature. There is a sequence of purely imaginary roots $\pm p_n$, $n = 1, 2, 3, \cdots$, which also imply the existence of evanescent modes. Similar observations were made by Maiti and Mandal (2014) in the case of a porous bed, and by Fox and Squire (1994) in the case of a non-porous bed. On the other hand, Fig. 3 reveals that when the porous-effect parameter G is complex, all the roots of the dispersion relations in open water and plate covered regions are complex in nature and all the roots are in close proximity with the roots discussed in Fig. 2 and the forms of the velocity potentials will remain similar to that of the real valued G as in Eq. (18). Moreover, it may be noted that the roots of the dispersion relation which are close to the real axis are referred as the most predominant progressive wave modes as discussed in Behera and Sahoo (2014). These modes are considered in the radiation condition as in Eq. (15) to account for the wave motion in regions I and 3.

Next, using the matching conditions at $x = 0$ and $x = b$ as in Eq. (11), and the orthogonality of the eigenfunctions as defined in Eq. (23), and truncating the infinite sums after $\mathbb{N}$ terms, a system of $4\mathbb{N} + 4$ equations for the determination of the unknowns associated with the velocity potentials in Eq. (18) are obtained as follows:

$$\sum_{n=0}^{\mathbb{N}} R_n X_{nm} - \sum_{n=0}^{\mathbb{N}} \left(A_n + B_n e^{-\mathrm{i}Q_n b}\right) Y_{nm} = -\delta_{0m} I_0 X_{0m}, \tag{24}$$

$$\sum_{n=0}^{\mathbb{N}} q_n R_n X_{nm} - \sum_{n=0}^{\mathbb{N}} Q_n \left(-A_n + B_n e^{-\mathrm{i}Q_n b}\right) Y_{nm} = \delta_{0m} q_0 I_0 X_{0m}, \tag{25}$$

$$\sum_{n=0}^{\mathbb{N}} T_n X_{nm} - \sum_{n=0}^{\mathbb{N}} \left(A_n e^{-\mathrm{i}Q_n b} + B_n\right) Y_{nm} = 0, \tag{26}$$

$$\sum_{n=0}^{\mathbb{N}} q_n T_n X_{nm} - \sum_{n=0}^{\mathbb{N}} Q_n \left(A_n e^{-\mathrm{i}Q_n b} - B_n\right) Y_{nm} = 0, \tag{27}$$

where

$$X_{nm} = \int_0^H f_n(k_n, z) f_m(k_m, z)\, \mathrm{d}z \quad \text{and} \quad Y_{nm} = \int_0^H g_n(p_n, z) f_m(k_m, z)\, \mathrm{d}z. \tag{28}$$

Further, it is assumed that the edges of the floating elastic plate are simple-supported. Thus, using Eq.

(13), four additional equations are obtained as follows:

$$\sum_{n=0}^{\mathbb{N}} E_n p_n \left(A_n + B_n e^{\mathrm{i}Q_n b}\right) = 0, \tag{29}$$

$$\sum_{n=0}^{\mathbb{N}} E_n p_n \left(A_n e^{\mathrm{i}Q_n b} + B_n\right) = 0, \tag{30}$$

$$\sum_{n=0}^{\mathbb{N}} EI\left(Q_n^2 - \nu\mu_y^2\right) E_n p_n \left(A_n + B_n e^{\mathrm{i}Q_n b}\right) = 0, \tag{31}$$

$$\sum_{n=0}^{\mathbb{N}} EI\left(Q_n^2 - \nu\mu_y^2\right) E_n p_n \left(A_n e^{\mathrm{i}Q_n b} + B_n\right) = 0, \tag{32}$$

where

$$E_n = \frac{p_n \sinh p_n H - G\cosh p_n H}{p_n \cosh p_n H - G \sinh p_n H}. \tag{33}$$

Solving the system of equations as given in Eqs. (24)–(27) and (29)–(32) will determine the unknown constants R_n, A_n, B_n and T_n. Similarly, Eqs. (12) and (14) are used in the case of the floating plate having free or clamped edges, respectively.

2.3. Numerical results and discussion

In this subsection, the effects of various wave and structural parameters such as bed porosity and plate characteristics are investigated in a homogeneous fluid of uniform density by analyzing the reflection and transmission coefficients which are computed using MATLAB programs. These reflection and transmission coefficients will provide global information about the scattering and dissipation of wave energy by the floating plate in the presence of porous sea bed. Moreover, the role of compressive force and bed porosity on the phase and group velocity is analyzed to understand the general characteristics of wave motion. Unless stated otherwise, the following values of physical parameters are considered: $I_0 = 1$ m, $H = 5$ m, $T = 5$ sec, $b/H = 6$, $GH = 0.25 + 0.25\mathrm{i}$, $g = 9.81$ m/sec^2, $\theta = 20^\circ$, $\nu = 0.3$, $E = 5$ GPa, $d = 0.1$ m, and $N = \sqrt{EI\rho g}$. Once the unknowns are determined, the reflection, transmission and dissipation coefficients can be easily computed using the formulae

$$K_r = \left|\frac{R_0}{I_0}\right|, \quad K_t = \left|\frac{T_0}{I_0}\right| \qquad \text{and} \quad K_d = 1 - (K_r^2 + K_t^2). \tag{34}$$

In order to study the convergence of the infinite series, numerical values of reflection coefficients K_r are computed for different values of $\mathbb{N}$ and illustrated Table 1 for certain fixed values of $k_0 H$ where $\mathbb{N} = 0$ represents the progressive wave mode solution. Table 1 reveals that the numerical results converge up to 5 decimal accuracy for $\mathbb{N}$ larger than 15.

In Figs. 4(a, b), the phase velocity ω/p_0 and group velocity $d\omega/dp_0$ versus wave number p_0 are plotted, respectively, for different values of the porous-effect parameter GH and compressive force N in case of flexural-gravity wave motion over a porous bed. Figure 4(a) reveals that for $N = 2(EI\rho g)^{1/2}$, zero phase velocity occurs in case of each GH. This value of N is referred to as critical compressive force for which the frequency of the progressive wave vanishes as discussed in Mohapatra et al.

k_0H	$\mathbb{N} = 0$	$\mathbb{N} = 5$	$\mathbb{N} = 10$	$\mathbb{N} = 15$	$\mathbb{N} = 20$
0.5	0.1054654562	0.0975174512	0.0187597247	0.0149550168	0.0149531597
1	0.1256894521	0.1216475125	0.0497451254	0.0467584576	0.0467570250
1.5	0.3057845146	0.2847974554	0.2098546671	0.2060375481	0.2060336793
2	0.7425598442	0.6987455478	0.6274213978	0.6204253978	0.6204213978
2.5	0.6124577556	0.6845783214	0.5131488765	0.5030298457	0.5030246132
3	0.88546512422	0.8154872975	0.7106545842	0.7097811254	0.7937708676
3.5	0.90238714567	0.8625564865	0.8298451238	0.8262481548	0.8262448433
4	0.90635485154	0.8692546163	0.8261668923	0.8227569875	0.8227525427

Table 1 Convergence of the reflection coefficient K_r for different values of $\mathbb{N}$ and non-dimensional wave number k_0H for the floating plate having clamped edge with $E = 1$ GPa, $N = \sqrt{EI\rho g}$, $b/H = 6$, $GH = 0.5$ and $\theta = 20°$.

(2013) in case of rigid bed. However, phase velocity decreases with an increase in the values of the porous-effect parameter GH. On the other hand, from Fig. 4(b), it is observed that the group velocity is negative for $N = 2(EI\rho g)^{1/2}$, which indicates that the wave crest and wave group move in opposite direction. Further, for $p_0 = 0.069$ and $N = 2(EI\rho g)^{1/2}$, certain discontinuity in wave energy propagation is observed irrespective of GH and is similar to the observation made in Mohanty et al. (2014) for $GH = 0$, which ensures that the value of the critical compressive force is unaltered in the presence of the sea bed porosity. For critical compressive force $N = 2(EI\rho g)^{1/2}$, the group velocity does not exist mathematically (see Mohanty et al. 2014) and buckling occurs under such circumstances. This will lead to the discontinuity in the behavior of the propagation of flexural gravity waves. Similar observations were made by Schulkes et al. (1987). However, for $GH \neq 0$, the group velocity decreases with an increase in N below the critical compressive force limit. This may be due to the fact that critical value of the compressive force is a plate characteristics, while porous-effect parameter is a characteristic of the sea bed. The bed porosity will change the wave-induced response not the structural characteristics of the floating plate. Thus, in the present study, the values of compressive force N is restricted to values below the critical compressive force.

In Figs. 5(a, b), the reflection coefficient versus $\omega\sqrt{H/g}$ are plotted for different values of non-dimensional plate length b/H with $\theta = 0°$ and $30°$, respectively, in case of plate having free edge conditions. Both the figures reveals that the curves of reflection coefficients K_r obtained by the present theory for rigid bed $GH = 0$ are in close agreement with Fig. 2 of Sturova (1999). Moreover, with an increase in non-dimensional plate length b/H, the number of zeros in wave reflection increases. A comparison between Figs. 5(a) and (b) reveals that there is a decrease in the frequency of occurrence of zero reflection for oblique angle of incidence. Further, for smaller plate length, wave reflection is less for oblique angle of incidence.

In Fig. 6(a), the reflection and transmission coefficients versus non-dimensional plate length k_0b are plotted for different edge conditions, namely; clamped, simply-supported and free edges. Figure 6(a) reveals that the plate having clamped edges exhibits larger reflection and smaller transmission which indicates that a major part of the wave energy will be reflected in case of a clamped edge plate and thus

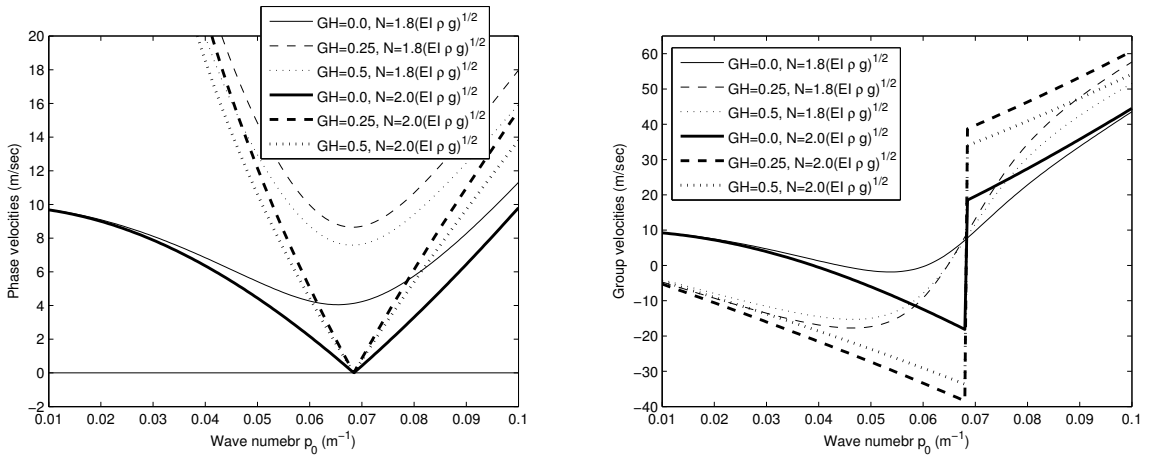

(a) (b)

Figure 4 Variation of (a) phase velocity and (b) group velocity versus wave number for different values of GH and N with $H = 10$ m and $E = 5$ GPa.

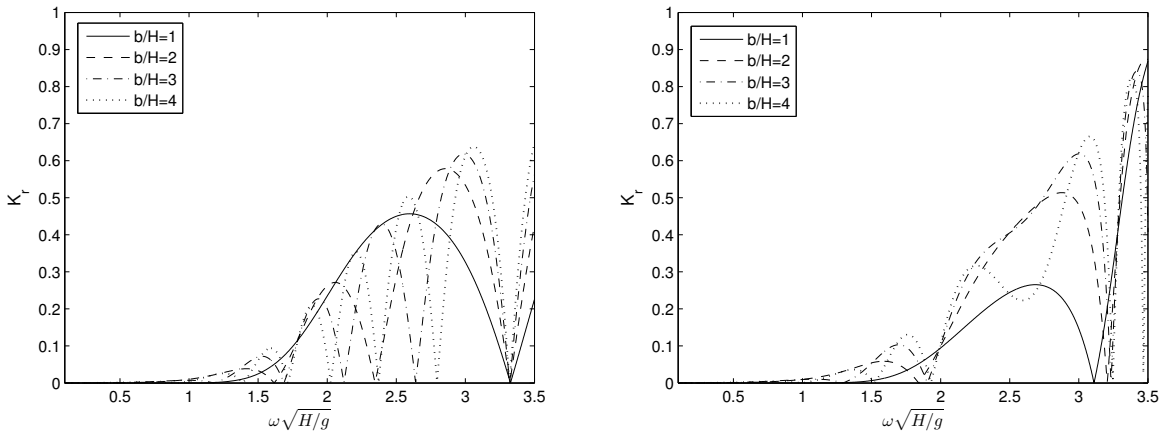

(a) (b)

Figure 5 Variation of the reflection coefficient versus $\omega\sqrt{H/g}$ for (a) $\theta = 0°$ and (b) $\theta = 30°$ with $E = 6$ GPa, $H = 100$ m, $d = 1$ m, $N = 0$ and $GH = 0$.

less wave will transmit below the plate. However, plate having free edges exhibits smaller reflection and larger transmission compared to the other two types of edge conditions. Thus, in case of a floating plate with free edge, wave-induced force on the floating plate will be more as more wave energy will transmit through the structure compared to that a plate having clamped or simply-supported edge. The dissipation coefficient versus $k_0 b$ is plotted for different edge conditions in Fig. 6(b). Figure 6(b) depicts that wave energy dissipates more with increase in plate length. Both the figures reveal that the reflection, transmission and dissipation coefficients follow certain oscillatory pattern with an increase in the structural length. Moreover, the study reveals that the amplitude of oscillation decrease with an increase in non-dimensional length $k_0 b$ as energy loss takes place by the porous bed. As it is found

that the plate having clamped edges results more reflection and less transmission, clamped edge may be preferred as an effective edge condition. Hereafter, all the numerical results in the manuscript are discussed for a floating plate having clamped edges.

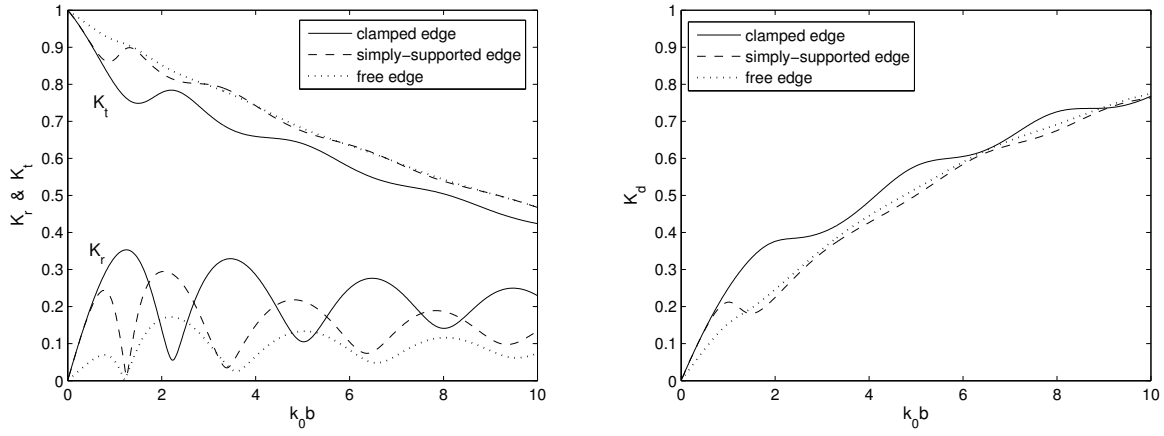

Figure 6 Variation of the (a) reflection and transmission coefficients (b) dissipation coefficients versus k_0b for different edge conditions with $GH = 0.25 + 0.25$i, $E = 1$ GPa, $N = \sqrt{EI\rho g}$ and $\theta = 20°$.

In Fig. 7(a), the reflection and transmission coefficients and (b) dissipation coefficients versus k_0b are plotted for different values of the porous-effect parameter GH. Figure 7(a) reveals that in case of non-porous bed ($GH = 0$) and real GH , the reflection and transmission coefficients follow certain oscillatory pattern, and zero reflection and full transmission observed periodically, and satisfies the energy relation $K_2^2+K_t^2 = 1$. On the other hand, for complex values of the porous-effect parameter GH, $K_2^2 + K_t^2 < 1$ due to the dissipation of wave energy by the porous bed. Moreover, in case of complex GH, with an increase in non-dimensional length of the plate k_0b, the amplitude of the oscillation of the reflection coefficient decreases uniformly with an increase in plate length. The uniform decrease in wave reflection is due to the dissipation of wave energy by the porous sea bed. Moreover, wave reflection and transmission decrease with an increase in the absolute value of GH in case of complex GH. Figure 7(b) reveals that the dissipation coefficient K_d increases with an increase in the absolute value of the porous-effect parameter GH and plate length which is due to the dissipation of wave energy as it passes through the porous bed.

In Figs. 8(a, b), the reflection and transmission coefficients versus non-dimensional plate length k_0b are plotted for different values of Young's modulus of the floating plate E and compressive force N respectively. Figure 8(a) depicts that the increase in Young's modulus of the plate E results in an increase in the wave reflection but a decrease in the wave transmission. The plate becomes more rigid with larger EI, and therefore most of the waves which concentrate near the free surface are reflected back and in the process less wave energy is transmitted below the plate. Similar observations were made by Sahoo et al. (2001) and Maiti and Mandal (2014) in the case of wave scattering by a semi-infinite plate over a porous/non-porous bed. Thus, the plate having a moderate value of E are suitable

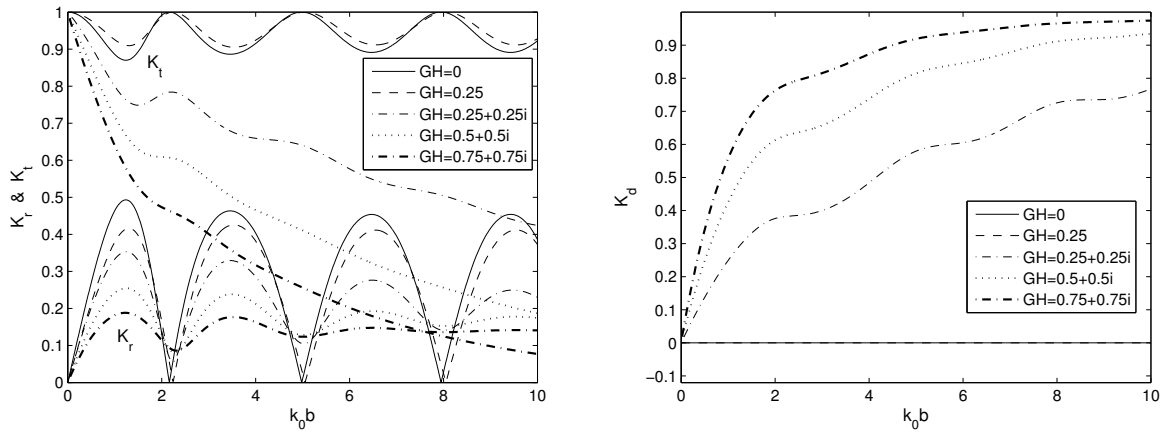

(a) (b)

Figure 7 Variation of the (a) reflection and transmission coefficients and (b) dissipation coefficients versus k_0b for different values of GH with clamped edge condition, $E = 1$ GPa, $N = \sqrt{EI\rho g}$ and $\theta = 20°$.

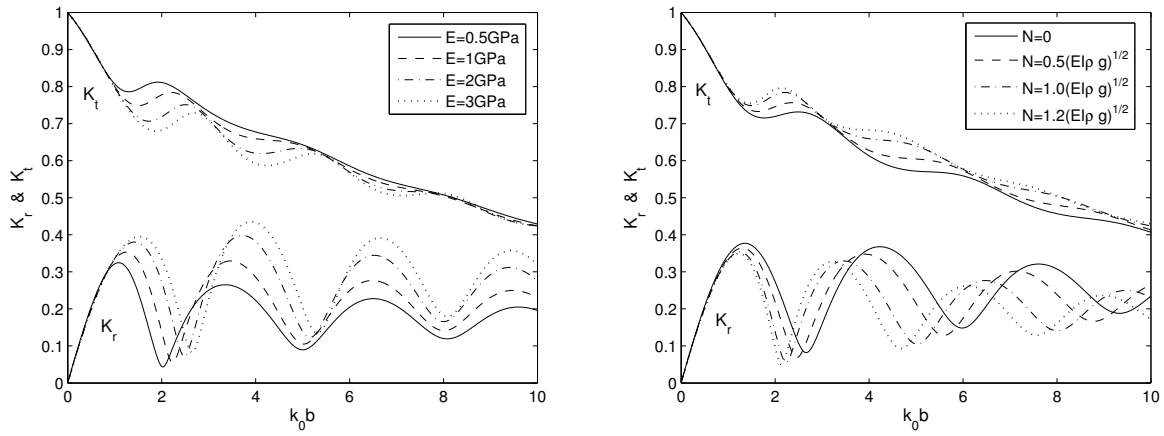

(a) (b)

Figure 8 Variation of the reflection and transmission coefficients versus k_0b for different values of (a) E with $N = \sqrt{EI\rho g}$ and (b) N with $E = 1$ GPa, and $GH = 0.25 + 0.25$i and $\theta = 20°$.

as an effective coastal structure for wave attenuation. On the other hand, the wave reflection decreases and transmission increases with an increase in compressive force N as shown Fig. 8(b). An increase in compressive force often enhances the structural deformation which result in the increase in the wave transmission and decrease in wave reflection within the critical limit. This may be due to the decay in the rate of energy propagation by the floating plate with an increase in compressive force as observed in Fig. 4.

In Figs. 9(a, b), the reflection and transmission coefficients versus oblique angle θ are plotted for different values of the porous-effect parameter GH and Young's modulus E of the floating plate respectively. Fig. 9(a) reveals that zero reflection and full transmission occur for certain values of the

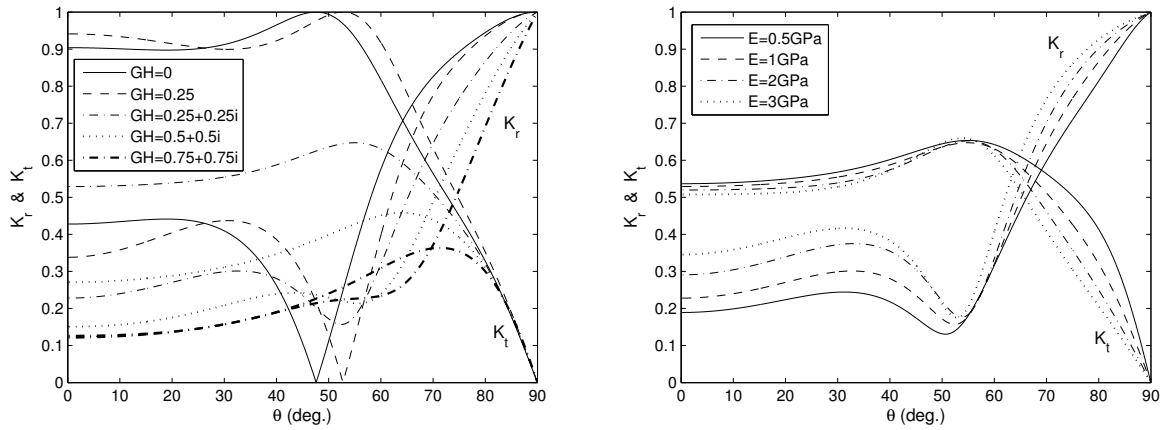

(a) (b)

Figure 9 Variation of the reflection and transmission coefficients versus θ for different values of (a) GH with $E = 1$ GPa and (b) E with $GH = 0.25 + 0.25$i, and $N = \sqrt{EI\rho g}$ and $b/H = 6$.

angle of incidence θ in case of non-porous bed ($GH = 0$) and real GH, and this angle is said to be the critical angle which is similar to the observation found in Behera et al. (2013) and Fox and Squire (1994). However, zero reflection and full transmission do not occur for complex GH. On the other hand, with an increase in the absolute value of the complex porous-effect parameter, there is an increase in the value of the angle of incidence for which wave reflection attends certain minimum which is due to the dissipation of wave energy by the porous bed. Figure 9(b) depicts that the reflection coefficient increases with an increase in Young's modulus E, while an opposite pattern is observed in the transmission coefficient which is similar to be observation found in Fig. 8(a).

3. Wave scattering by a floating elastic plate in a two-layer fluid system

In this subsection, the problem for wave scattering by a floating elastic plate in a two-layer fluid over a porous bed is presented. Unlike the case of a single-layer fluid, due to the presence of the interface and the free surface and plate covered surface, there exist two wave modes in each of the open water regions and plate covered region as discussed in Behera et al. (2013) and Bhattacharjee and Sahoo (2008).

3.1. Mathematical Formulation

In this case, the fluid and structural characteristics are the same as have been considered in subsection 2.1 except that the fluid domain is occupied by two immiscible fluids having the mean interface at $z = h$. The upper and lower fluids are of finite depths $0 < z < h$ and $h < z < H$, and constant densities ρ_1 and ρ_2, respectively as shown in Fig. 10. The velocity potentials Φ_j for $j = 1, 2, 3$ satisfy Eq. (1) along with the boundary conditions (2)–(8) with ρ being replaced by ρ_1. Further, using the continuity of velocity and pressure at the interface, the dynamic and boundary conditions at the mean interface at $z = h$ yield (as in Bhattacharjee and Sahoo (2008))

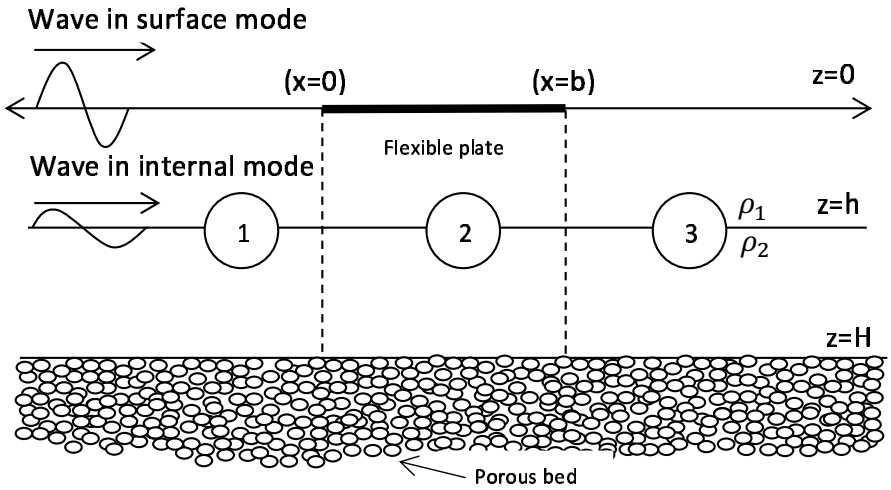

Figure 10 Schematic diagram of wave scattering by floating elastic plate over a porous bed in two-layer fluid.

$$\left.\frac{\partial \Phi_j}{\partial z}\right|_{z=h^-} = \left.\frac{\partial \Phi_j}{\partial z}\right|_{z=h^+} = \frac{\partial \xi_j}{\partial t} \quad \text{for } j = 1, 2, 3, \tag{35}$$

$$s\left(\frac{\partial \Phi_j}{\partial t} - g\xi_j\right)\Big|_{z=h^-} = \left(\frac{\partial \Phi_j}{\partial t} - g\xi_j\right)\Big|_{z=h^+} \quad \text{for } j = 1, 2, 3, \tag{36}$$

where ξ_j for $j = 1, 2, 3$ are the interface elevations in regions 1, 2, 3, respectively, and $s = \rho_1/\rho_2$ with $0 < s < 1$. Moreover, the spatial velocity potential satisfy the Helmholtz equation as in Eq. (9), along with the boundary conditions given in Eqs. (10)–(14). Now, the radiation condition for oblique wave scattering by a floating elastic plate in a two-layer fluid over porous bed gives

$$\phi_j(x,z) = \begin{cases} \displaystyle\sum_{n=I}^{II} \left(I_n e^{iq_n x} + R_n e^{-iq_n x}\right) f_n(k_n, z), & j = 1, x \to -\infty, \\ \displaystyle\sum_{n=I}^{II} T_n e^{iq_n x} f_n(k_n, z), & j = 3, x \to \infty, \end{cases} \tag{37}$$

where I_n, R_n and T_n for $n = I, II$ are constants associated with the incident, reflected, and transmitted wave amplitudes, respectively, in the surface and internal modes, with $q_n = \sqrt{k_n^2 - \mu_y^2}$. Here, k_I and k_{II} are the complex wave numbers associated with the most predominant progressive waves surface mode (SM) and the internal mode (IM) in the open-water regions 1 and 3 respectively with $f_n(k_n, z)$ being the associated eigenfunctions. Details about the roots of the dispersion relation will be discussed in the subsequent Section.

3.2. Method of solution

For analyzing the role of wave motion in the two-layer fluid domain, it is assumed that the plane progressive flexural gravity waves in the surface and internal modes are of the forms $\eta = \mathrm{Re}\{\eta_0 e^{\mathrm{i}(px-\omega t)}\}$ and $\zeta = \mathrm{Re}\{\zeta_0 e^{\mathrm{i}(px-\omega t)}\}$ with η_0 and ζ_0 being the amplitudes of the flexural gravity waves in the surface and internal modes, respectively. Using the governing equation (1) along with boundary

conditions (2)–(4) and (35)–(36), the velocity potential can be written as

$$\Phi(x,z,t) = \begin{cases} \dfrac{-\mathrm{i}\omega(\mu\cosh pz + \sinh pz)\eta}{p}, & 0 < z < h, \\ \dfrac{\mathrm{i}\omega\{p\cosh p(H-z) - G\sinh p(H-z)\}\zeta}{p\{p\sinh p(H-h) - G\cosh p(H-h)}, & h < z < H, \end{cases} \tag{38}$$

where G is the porous-effect parameter associated with the porous bed as discussed in Section 2, and p is the wave number of the gravity waves in the plate-covered region which satisfies the dispersion relation

$$K(Mp - \mu) = p(Dp^4 - Qp^2 + 1). \tag{39}$$

In Eq. (39), μ is given by

$$\mu = -\frac{\{(s\tanh ph + L)K - (1-s)p\}\coth ph}{(s\coth ph + L)K - (1-s)p}, \tag{40}$$

where

$$L = \frac{p\coth p(H-h) - G}{p - G\coth p(H-h)}. \tag{41}$$

Also, the ratio of the amplitudes of flexural gravity waves in the surface and internal modes is given by

$$\frac{\eta_0}{\zeta_0} = \frac{\{s\coth ph + L\}K - p(1-s)}{sK}. \tag{42}$$

An equivalent form of Eq. (39) is given by

$$U_p K^2 - V_p K + W_p = 0, \tag{43}$$

where

$$\begin{aligned} U_p &= (Mp - \tilde{G}s)\coth p(H-h) + (Mps - \tilde{G})\coth ph + (1 - \tilde{G}Ms)\coth p(H-h)\coth ph \\ &\quad + (s - \tilde{G}M), \\ V_p &= p[\{C - \tilde{G}M(1-s)\}\coth p(H-h) + Z\{\coth ph - \tilde{G}\coth p(H-h)\coth ph\} \\ &\quad + pM(1-s) - \tilde{G}C], \\ W_p &= p^2C(1-s)\{1 - \tilde{G}\coth p(H-h)\}, \end{aligned}$$

with $\tilde{G} = G/p$, $Z = s(C-1) + 1$, $C = Dp^4 - Qp^2 + 1$ and $M = \rho_s d/\rho_1$. On the other hand, for $D = 0$, $Q = 0$ and $M = 0$, Eqs. (42) and (43) give the amplitude ratio and dispersion relation for the open-water region in the presence of a porous bed, and the dispersion relation in the open-water region in terms of k is given by

$$U_w K^2 - V_w K + W_w = 0, \tag{44}$$

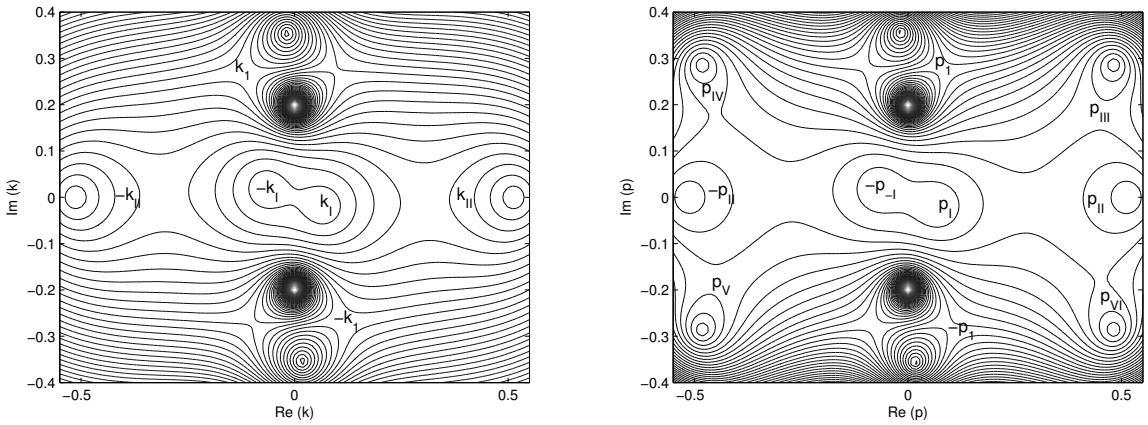

(a) (b)

Figure 11 Contour plots of roots of the dispersion relation for (a) open-water region and (b) plate-covered region in two-layer fluid over porous bed with $H = 10$m, $s = 0.75$, $h/H = 0.2$, $T = 8$sec., $g = 9.81$m/sec^2, $\nu = 0.3$, $GH = 0.5 + 0.5$i, $E = 1$GPa, $d = 0.1$ and $Q = 0.5\sqrt{EI\rho g}$.

where

$$U_w = s + \coth k(H-h)\coth kh - \tilde{G}\{s\coth k(H-h) + \coth kh\},$$
$$V_w = k[\coth k(H-h) + \coth kh - \tilde{G}\{\coth k(H-h)\coth kh + 1\}],$$
$$W_w = k^2(1-s)\{1 - \tilde{G}\coth k(H-h)\}.$$

It may be noted that for $G = 0$ and $Q = 0$, the dispersion relation in Eqs. (43) and (44) reduce to the dispersion relations for the open-water and plate-covered regions, respectively, in a two-layer fluid over a non-porous bed, as in Lin and Lu (2013). Further, for $Q = 0$, $s = 1$ and $h \to H$, the dispersion relations in Eqs. (43) and (44) reduce to the corresponding dispersion relations in the case of a single-layer fluid as given in Eqs. (21) and (22), respectively. In a manner similar to that for a single-layer fluid as described in subsection 2.1, the roots of the dispersion relations for open-water and plate-covered regions, as given in Eqs. (43) and (44), are shown in Figs. 11(a, b), respectively. Unlike gravity wave motion over a non-porous bed, Fig. 11(a) reveals that the dispersion relation in Eq. (43) has two pairs of complex roots of opposite signs $\pm k_I$ and $\pm k_{II}$, which are referred to as the wave numbers associated with the most predominant progressive waves in surface mode (SM) and internal mode (IM), respectively. Further, it has infinitely many complex roots which are close to the imaginary axis with opposite signs $\pm k_n$, $n = 1, 2, 3, \cdots$ and correspond to the evanescent modes. On the other hand, unlike flexural gravity wave motion over an impermeable bed, Fig. 11(b) shows that the dispersion relation given in Eq. (44) has two pairs of complex roots of opposite signs $\pm p_I$ and $\pm p_{II}$ and are referred to as the wave numbers associated with the most predominant progressive waves in the flexural gravity mode and internal mode and are very close to the real−axis, two pairs of complex roots of the forms $p_{III} = \bar{p}_{VI}$ and $p_{IV} = \bar{p}_V$, which are non-propagating in nature and lies in the complex plane and there are a sequence of complex roots $\pm p_n$, $n = 1, 2, 3, \cdots$, which are

close to the imaginary axis and corresponds to the evanescent modes (similar to Behera and Sahoo (2014)). Moreover, similar observations were made by Bhattacharjee and Sahoo (2008) for a non-porous bed where the wave number associated with the progressive wave mode is a real number and evanescent wave modes are purely imaginary numbers. Thus, in a two-layer fluid, the forms of the spatial velocity potentials in regions 1, 2 and 3 are given by

$$\phi_j(x,z) = \begin{cases} \sum_{n=\mathrm{I}}^{\mathrm{II}} I_n \mathrm{e}^{\mathrm{i}q_n x} f_n(k_n,z) + \sum_{n=\mathrm{I,II,1}}^{\infty} R_n \mathrm{e}^{-\mathrm{i}q_n x} f_n(k_n,z), & \text{for} \quad x<0, j=1, \\ \sum_{n=\mathrm{I,II,1}}^{\infty} \left\{A_n \mathrm{e}^{\mathrm{i}Q_n x} + B_n \mathrm{e}^{-\mathrm{i}Q_n(x-b)}\right\} g_n(p_n,z), & \text{for} \quad 0<x<b, j=2, \\ \sum_{n=\mathrm{I,II,1}}^{\infty} T_n \mathrm{e}^{\mathrm{i}q_n(x-b)} f_n(k_n,z), & \text{for} \quad x>b, j=3, \end{cases} \tag{45}$$

where R_n, A_n, B_n and T_n for $n = I, II, 1, 2, \cdots$ are the unknown coefficients to be determined, I_ns are associated with the amplitudes of the incident waves in surface and internal modes and are assumed to be known. Moreover, R_n and T_n for $n = I$ and II are associated with the amplitudes of the reflected and transmitted waves in surface and internal modes respectively. In Eq. (45), k_n and p_n are the roots of the dispersion relation as given in Eq. (43) and (44), respectively with $q_n = \sqrt{k_n^2 - \mu_y^2}$ and $Q_n = \sqrt{p_n^2 - \mu_y^2}$. Further, the eigenfunctions $f_n(k_n,z)$ and $g_n(k_n,z)$ are given by

$$f_n(k_n,z) = \begin{cases} -\left[\dfrac{\sinh k_n(H-h) - \tilde{G}\cosh k_n(H-h)}{k_n \sinh k_n h - K\cosh k_n h}\right](k_n \cosh k_n z - K \sinh k_n z), & 0<z<h, \\ \cosh k_n(H-z) - \tilde{G}\sinh k_n(H-z), & h<z<H, \end{cases} \tag{46}$$

$$g_n(p_n,z) = \begin{cases} -\left[\dfrac{\sinh p_n(H-h) - \tilde{G}\cosh p_n(H-h)}{p_n \tilde{C} \sinh p_n h - K\cosh p_n h}\right](p_n \tilde{C} \cosh p_n z - K \sinh p_n z), & 0<z<h, \\ \cosh p_n(H-z) - \tilde{G}\sinh p_n(H-z), & h<z<H, \end{cases} \tag{47}$$

where $\tilde{C} = C - MK$, and C, M and $\tilde{G}$ are the same as those defined in Eq. (43). The eigenfunctions $f_n(k_n,z)$ in the open-water region is integrable in $0 < z < H$ having a discontinuity at $z = h$ and are orthogonal with respect to the inner product defined by

$$\langle f_n(k_n,z), f_m(k_m,z)\rangle = s\int_0^h f_n(k_n,z) f_m(k_m,z)\,\mathrm{d}z + \int_h^H f_n(k_n,z) f_m(k_m,z)\,\mathrm{d}z. \tag{48}$$

Again, in a manner similar to that in the case of a single-layer fluid, a system of equations for the determination of the unknowns associated with the velocity potentials in Eq. (45) are obtained as

follows:

$$\sum_{n=I,II,1}^{\mathbb{N}} R_n X_{nm} - \sum_{n=n=I,II,1}^{\mathbb{N}} \left(A_n + B_n e^{-\mathrm{i}Q_n b}\right) Y_{nm} = -\sum_{n=I}^{II} \delta_{nm} I_n X_{nm}, \tag{49}$$

$$\sum_{n=I,II,1}^{\mathbb{N}} q_n R_n X_{nm} - \sum_{n=I,II,1}^{\mathbb{N}} Q_n \left(-A_n + B_n e^{-\mathrm{i}Q_n b}\right) Y_{nm} = \sum_{n=I}^{II} \delta_{nm} q_n I_n X_{nm}, \tag{50}$$

$$\sum_{n=I,II,1}^{\mathbb{N}} T_n X_{nm} - \sum_{n=I,II,1}^{\mathbb{N}} \left(A_n e^{-\mathrm{i}Q_n b} + B_n\right) Y_{nm} = 0, \tag{51}$$

$$\sum_{n=I,II,1}^{\mathbb{N}} q_n T_n X_{nm} - \sum_{n=I,II,1}^{\mathbb{N}} Q_n \left(A_n e^{-\mathrm{i}Q_n b} - B_n\right) Y_{nm} = 0, \tag{52}$$

where δ_{nm} is the Kronecker delta, and $m = I, II, 1, 2, \cdots$, with

$$X_{nm} = s \int_0^h f_n(k_n, z) f_m(k_m, z)\, \mathrm{d}z + \int_h^H f_n(k_n, z) f_m(k_m, z)\, \mathrm{d}z, \tag{53}$$

and

$$Y_{nm} = s \int_0^h g_n(p_n, z) f_m(k_m, z)\, \mathrm{d}z + \int_h^H g_n(p_n, z) f_m(k_m, z)\, \mathrm{d}z. \tag{54}$$

Further, as has been discussed for a single-layer fluid, the plates has to satisfy one of the edge conditions namely free, simply supported or built-in edge. In the context of the present Section, it is assumed that the plate is having simply-supported edges. Thus, using Eq. (13), four additional equations are obtained as below:

$$\sum_{n=I,II,1}^{\mathbb{N}} KE_n p_n \left(A_n + B_n e^{\mathrm{i}Q_n b}\right) = 0, \tag{55}$$

$$\sum_{n=I,II,1}^{\mathbb{N}} KE_n p_n \left(A_n e^{\mathrm{i}Q_n b} + B_n\right) = 0, \tag{56}$$

$$\sum_{n=I,II,1}^{\mathbb{N}} EI(Q_n^2 - \nu\mu_y^2) KE_n p_n \left(A_n + B_n e^{\mathrm{i}Q_n b}\right) = 0, \tag{57}$$

$$\sum_{n=I,II,1}^{\mathbb{N}} EI(Q_n^2 - \nu\mu_y^2) KE_n p_n \left(A_n e^{\mathrm{i}Q_n b} + B_n\right) = 0, \tag{58}$$

where

$$E_n = \frac{\sinh p_n(H-h) - \tilde{G}\cosh p_n(H-h)}{p_n \tilde{C} \sinh p_n h - K \cosh p_n h}. \tag{59}$$

Next, to determine the unknown constants R_n, A_n, B_n and T_n for $n = I, II, 1, 2, \cdots$, Eqs. (49)–(52) and (55)–(58) are solved. Similarly, Eqs. (12) and (14) are used in the case of the floating plate having free and clamped edges respectively.

3.3. Numerical results and discussion

In this case, the depth ratio $h/H = 0.2$, density ratio $s = 0.75$ and other parameters given in the subsection 2.3 are kept fixed unless it is stated otherwise. The reflection and transmission coefficients in SM and IM can be easily computed using the formulae

$$\left.\begin{aligned} K_{rI} &= \left|\frac{R_I}{I_I}\right| \quad \text{and} \quad K_{tI} = \left|\frac{T_I}{I_I}\right| \quad \text{in SM,} \\ K_{rII} &= \left|\frac{R_{II}}{I_{II}}\right| \quad \text{and} \quad K_{tII} = \left|\frac{T_{II}}{I_{II}}\right| \quad \text{in IM.} \end{aligned}\right\} \tag{60}$$

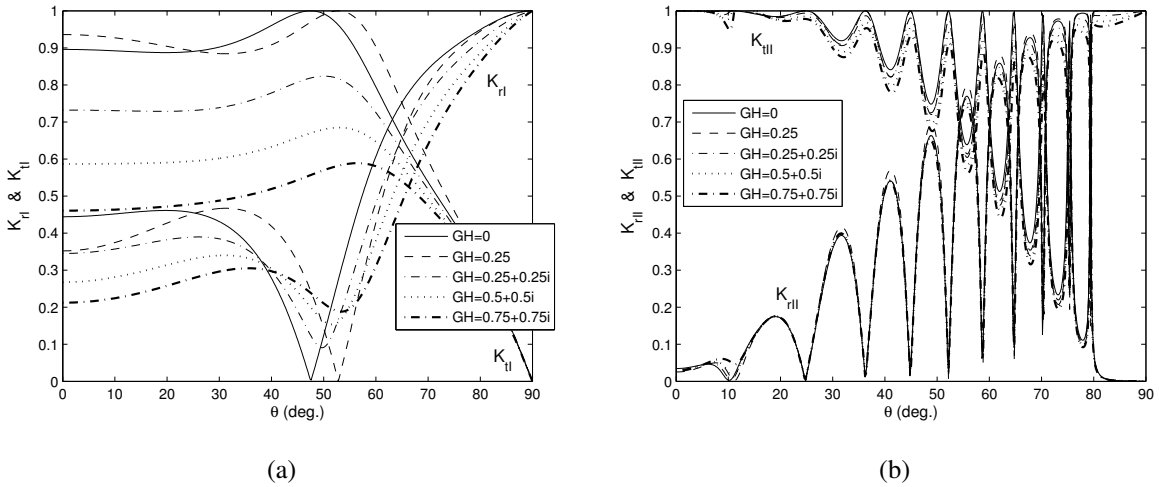

(a) (b)

Figure 12 Variation in reflection and transmission coefficients versus oblique angle θ in (a) SM and (b) IM for different values of GH with $h/H = 0.25$, $s = 0.75$ and $b/H = 6$.

In Figs. 12(a, b), the reflection and transmission coefficients versus oblique angle θ are plotted for waves in SM and IM, respectively, for different values of the porous-effect parameter GH. Figure 12(a) depicts that with an increase in the absolute value of the porous-effect parameter GH results lower reflection and transmission in SM. Further, in SM, zero reflection and full transmission occur for certain values of the angle of incidence θ in case of rigid bottom ($GH = 0$) and real GH. Similar observation is obtained for a homogeneous fluid as has been shown in Fig. 9(a). Moreover, zero minimum in the reflection coefficient for waves in surface mode does not occur for complex porous effect parameter GH and the observation is similar to that of a homogeneous fluid. Moreover, increasing absolute values of GH tends to shift the position of the minimum reflection for waves in SM. Figure 12(b) depicts that with an increase in the oblique angle of incidence, frequency of occurrence of zero wave reflection in internal mode increases and amplitude of oscillation in wave reflection increases with an increase in angle of incidence which may be due to the resonating interaction of the waves in surface and internal modes. The maxima in wave reflection corresponds to the case of constructive interference, while the minima corresponds to the case of destructive interference. Further, the wave reflection and transmission decrease in IM with an increase in the absolute values of GH. The variations in wave reflection and transmission for waves in IM compared to that in SM with an increase in

the porous-effect parameter is due to the fact that in a two-layer fluid system, the angle of incidence in surface mode and internal modes changes with stratification which follows Snell's law of refraction.

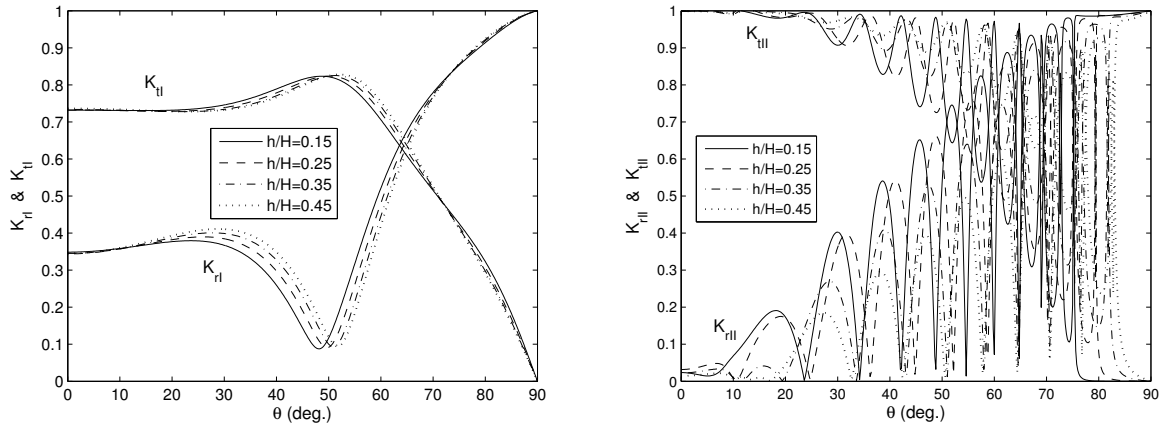

(a) (b)

Figure 13 Variation in reflection and transmission coefficients versus oblique angle θ in (a) SM and (b) IM for different values of h/H with $GH = 0.25 + 0.25\mathrm{i}$, $s = 0.75$ and $b/H = 6$.

In Figs. 13(a, b), the reflection and transmission coefficients versus oblique angle θ are plotted for waves in SM and IM, respectively, for different values of the depth ratio h/H. Both the figures demonstrates that the general patterns in wave reflection and transmission are similar to those discussed above in Figs. 12(a, b). Owing to the higher wave energy concentration near the free surface, the wave reflection is more and wave transmission is less in both SM and IM when the interface is closer to the free surface. Similar observation was made by Behera et al. (2015) in the case of wave scattering by a partial porous structure in a two-layer fluid. Figure 13(a) depicts that with an increase in h/H, zero reflection and full transmission occur for lower values of oblique angle θ.

In Figs. 14(a, b), the reflection and transmission coefficients versus oblique angle θ are plotted for waves in SM and IM, respectively, for different values of the density ratio s. From these figures, it is observed that the reflection coefficient decreases while the transmission coefficient increases as the density ratio s increases. This may be sue to the fact that as the density variation increases interfacial effect becomes more predominant and the role of waves in interface plays a significant role which obstruct the wave motion. Figure 14(b) depicts that oscillatory patterns in wave reflection and transmission for waves in IM increases with an increase in the density ratio s which is due to the mutual interaction between waves in surface and interface.

In Figs. 15(a, b), the reflection and transmission coefficients versus oblique angle θ are plotted for waves in SM and IM, respectively, for different values of Young's modulus of the floating plate E. From Fig. 15(a), it is observed that the wave reflection increases while the wave transmission decreases with an increase in Young's modulus of the plate E. This is similar to the case of homogeneous fluid as has been seen in Fig. 7(b). On the other hand, Fig. 15(b) depicts that the wave reflection

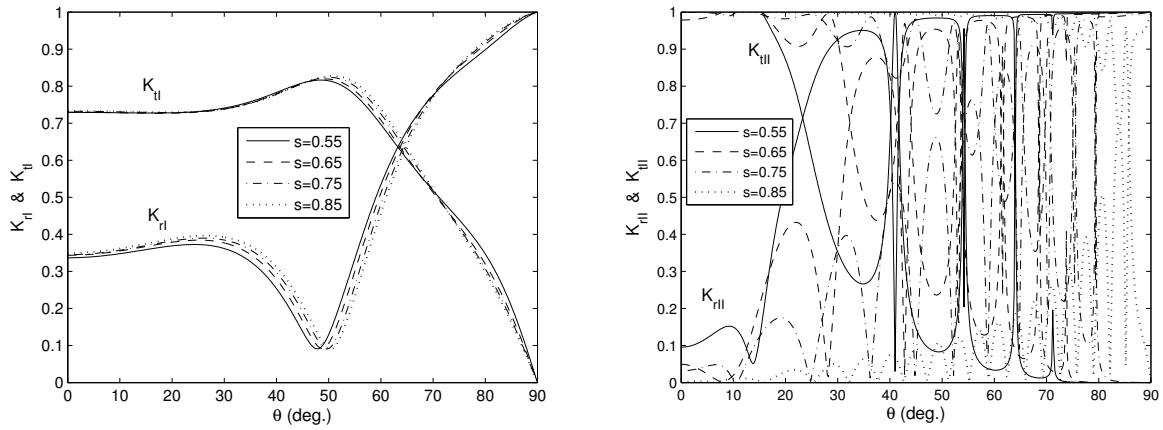

(a) (b)

Figure 14 Variation in reflection and transmission coefficients versus oblique angle θ in (a) SM and (b) IM for different values of s with $GH = 0.25 + 0.25$i, $h/H = 0.25$ and $b/H = 6$.

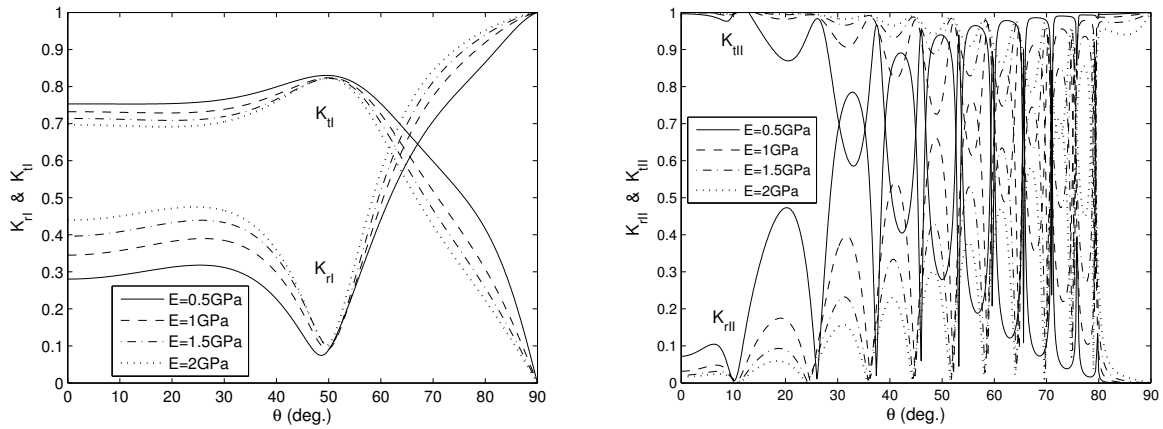

(a) (b)

Figure 15 Variation in reflection and transmission coefficients versus oblique angle θ in (a) SM and (b) IM for different values of E with $GH = 0.25 + 0.25$i, $h/H = 0.25$, $s = 0.75$ and $b/H = 6$.

decreases for IM waves with an increase in E.

In Figs. 16(a, b), the reflection and transmission coefficients versus oblique angle θ are plotted for waves in SM and IM, respectively, for different values of compressive force N. Figure 16(a) depicts that there are two times where minima of wave reflection occur in SM when compressive force tends to zero and $0 < \theta < 90°$, while for larger values of compressive force N, there is only one time where minimum of wave reflection occurs. However, the number of times where minima of reflection and maxima of transmission occur do not change with an increase in the compressive force, as shown in Fig. 16(b) for IM waves. Generally, K_{rI} increases and K_{tI} decreases as the compressive force increases, while K_{rII} decreases and K_{tII} increases as the compressive force N increases.

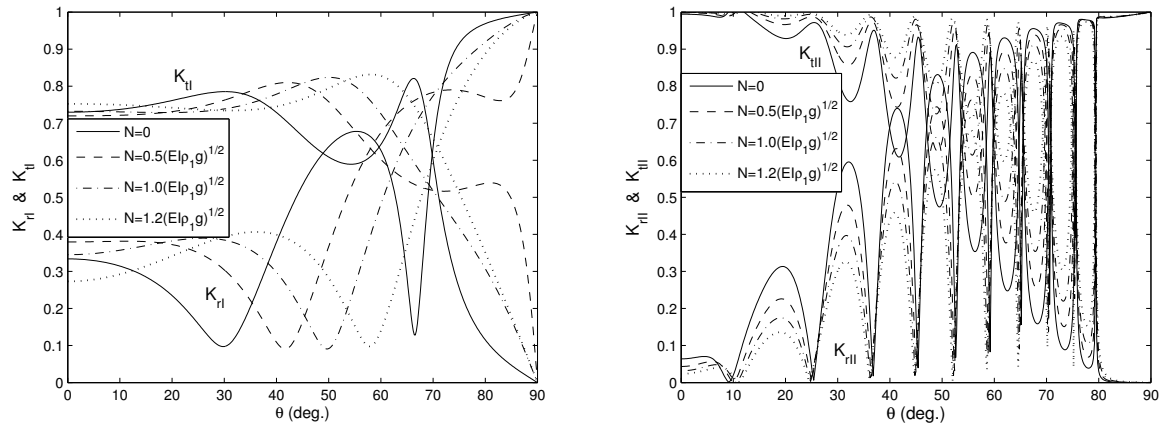

(a) (b)

Figure 16 Variation in reflection and transmission coefficients versus oblique angle θ in (a) SM and (b) IM for different values of N with $GH = 0.25 + 0.25\text{i}$, $h/H = 0.25$, $s = 0.75$ and $b/H = 6$.

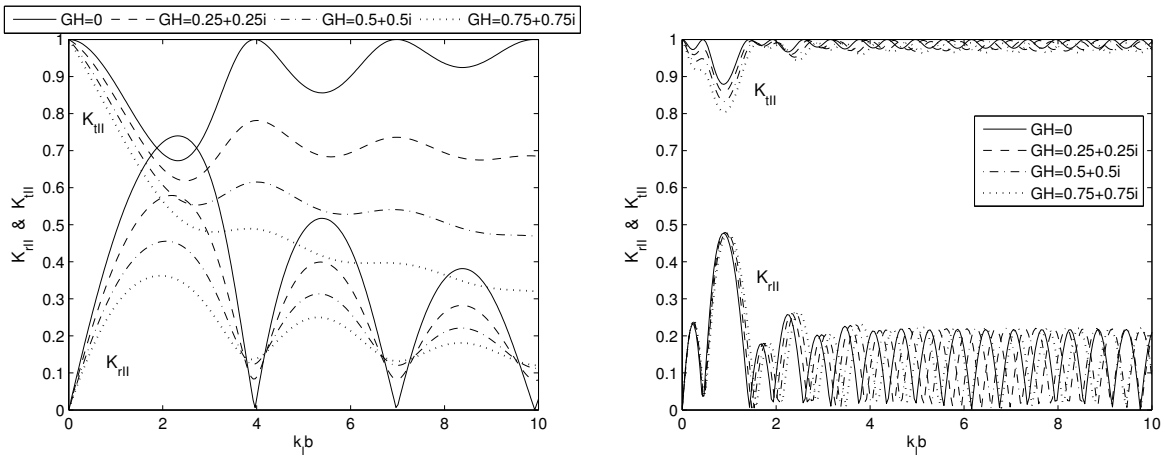

(a) (b)

Figure 17 Variation in reflection and transmission coefficients versus k_Ib in (a) SM and (b) IM for different values of GH with $\theta = 20°$, $h/H = 0.25$ and $s = 0.75$.

In Figs. 17(a, b), the reflection and transmission coefficients versus non-dimensional plate length k_Ib are plotted for waves in SM and IM, respectively, for different values of the porous-effect parameter GH. Figure 17(a) shows that both the wave reflection and transmission in SM decrease as a result of the increase in the absolute values of porous-effect parameter GH. Moreover, unlike the occurrence of multiple zeros in wave reflection for real value of porous-effect parameter, zero reflection does not occur for complex porous-effect parameter GH with an increase in plate length k_Ib. This is similar to that for homogeneous fluid, as seen in Fig. 7(a). On the other hand, wave reflection increases and wave transmission decreases for waves in IM with an increase in the absolute values of GH. In the two-layer fluid system, since the total wave energy is conserved, less energy concentration near the

free surface corresponds to higher energy concentration at the interface. Thus, due to the resonating interaction of the waves in SM and IM, waves in IM becomes predominant and is reflected by the floating plate.

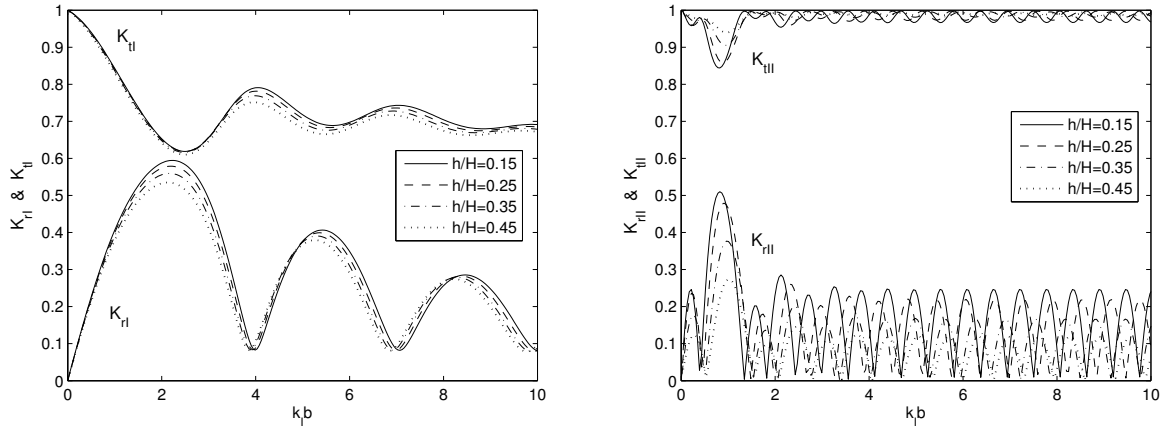

(a) (b)

Figure 18 Variation in reflection and transmission coefficients versus $k_I b$ in (a) SM and (b) IM for different values of h/H with $\theta = 20°$, $GH = 0.25 + 0.25$i and $s = 0.75$.

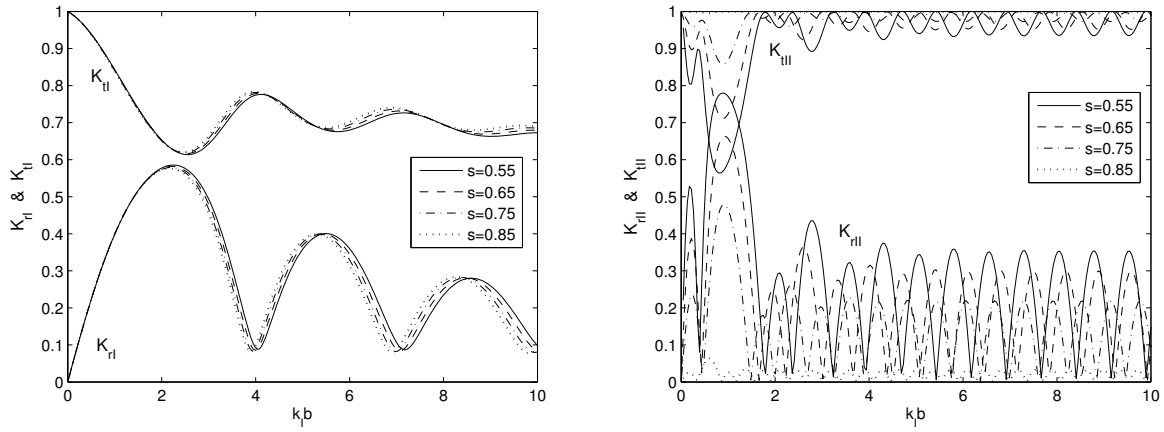

(a) (b)

Figure 19 Variation in reflection and transmission coefficients versus $k_I b$ in (a) SM and (b) IM for different values of s with $\theta = 20°$, $GH = 0.25 + 0.25$i and $h/H = 0.25$.

In Figs. 18(a, b), the reflection and transmission coefficients versus non-dimensional plate length $k_I b$ are plotted for waves in SM and IM, respectively, for different values of the depth ratio h/H. The general patterns in wave reflection and transmission for SM and IM waves are similar to those already observed in Figs. 17(a, b). Fig. 18(a) depicts that as the depth ratio h/H increases, the minima in the wave reflection for SM shifted to the left. However, Fig. 18(b) depicts that for waves in IM,

with an increase in h/H, the minima in the wave reflection shifted to the right. From these figures, it is observed that the amplitude of the oscillatory pattern of the reflection coefficient decreases with an increase in h/H. This is due to the concentration of higher amount of wave energy near the free surface as has been discussed in Behera et al. (2015). Like the earlier discussion, wave transmission follows an opposite trend to that of wave reflection for waves in SM and IM.

In Figs. 19(a, b), the reflection and transmission coefficients versus non-dimensional plate length $k_I b$ are plotted for waves in SM and IM, respectively, for different values of the density ratio s. In general, wave reflection decreases and the transmission increases for both SM and IM waves, with an increase in the density ratio s. The patterns in wave reflection and transmission are more oscillatory in IM when compared with that in SM. The optimum wave reflection is due to the constructive interference, while the minimum wave reflection is due to the destructive interference of the waves in SM and IM. Moreover, the increase in the frequency of occurrence of optimum wave reflection and transmission in IM is due to the resonating interaction of the waves in surface and internal modes. Figure 19(b) depicts that as with an increase in density ratio, smaller wave reflection and nearly full transmission occur for waves in IM. With an increase in the density ratio, the two fluid behaves like a single fluid and the role of the interface diminishes which results in the transmission of a major part of the wave energy with negligible reflection.

4. Conclusion

In the present paper, oblique wave scattering by a floating elastic plate over a porous bed is studied in single and two-layer fluid systems. The mathematical problems are formulated under the assumption of small-amplitude waves and structural response, and are solved using the eigenfunction expansion method. Numerical results are computed and discussed for the reflection and transmission coefficients to reveal effects due to the wave and structural parameters. The computed results are validated by comparing with known results available in the literature in both the cases of a single and two-layer fluids over a non-porous bed. Inclusion of the resistance effect in the porous-effect parameter leads to dissipation of global wave energy due to energy loss by porous sea bed. A comparison for various types of edge conditions reveals that in case of a floating plate with free edge, wave-induced force on the floating plate will be more as more wave energy will transmit through the structure compared to that a plate having clamped or simply-supported edge. It is depicted that the critical compressive force for which wave celerity vanishes in the plate covered region is independent of the bed permeability. However, for $GH \neq 0$, the group velocity decreases with an increase in the compressive force N below the critical compressive force limit. The present study depicts that under particular conditions for some combinations of the wave and structural parameters, zero reflection and full transmission may occur in case of rigid bottom and real GH for porous bed. However, for complex GH, zero reflection and full transmission do not occur. Moreover, in case of complex GH, due the energy dissipation by porous bed, wave transmission decreases significantly with increase in length of the floating plate. Further, the study reveals that with an increase in the absolute values of the porous-effect parameter of the porous bed, both wave reflection and transmission decrease in both the case of single and two-layer fluids. The patterns in the wave reflection and transmission in the

internal mode are more oscillatory when compared with that in the surface mode which is due to the resonating interaction of the waves in surface and interface modes. Due to the higher wave energy concentration near the free surface, wave reflection is larger and wave transmission is hence lower for waves in either the surface or internal mode when the interface is closer to the free surface. These findings will enhance the understanding of the wave energy distribution in a homogeneous and stratified fluid in oblique seas and will be of immense help in the design of floating breakwaters and other marine structures located on a porous sea bed. The concept can be generalized to include the role of bottom undulation for dealing with wave-structure interaction problems in the presence of porous bed.

References

Behera, H., Koley, S., Sahoo, T., 2015. Wave transmission by partial porous structures in two-layer fluid. Engineering Analysis with Boundary Elements 58, 58–78.

Behera, H., Mandal, S., Sahoo, T., 2013. Oblique wave trapping by porous and flexible structures in a two-layer fluid. Physics of Fluids 25, 112110.

Behera, H., Sahoo, T., 2014. Gravity wave interaction with porous structures in two-layer fluid. Journal of engineering mathematics 87, 73–97.

Belibassakis, K.A., 2012. Water-wave induced groundwater pressure and flow in variable bathymetry regions and sandy beaches by an enhanced coupled-mode model. Ocean Engineering 47, 104–118.

Bennetts, L.G., Williams, T.D., 2015. Water wave transmission by an array of floating discs, in: Proceedings of the Royal Society of London A: Mathematical, Physical and Engineering Sciences, The Royal Society. p. 20140698.

Bhattacharjee, J., Sahoo, T., 2008. Flexural gravity wave problems in two-layer fluids. Wave Motion 45, 133–153.

Chen, X.J., Wu, Y.S., Cui, W.C., Jensen, J.J., 2006. Review of hydroelasticity theories for global response of marine structures. Ocean Engineering 33, 439–457.

Dalrymple, R.A., Losada, M.A., Martin, P.A., 1991. Reflection and transmission from porous structures under oblique wave attack. Journal of Fluid Mechanics 224, 625–644.

Fox, C., Squire, V.A., 1990. Reflection and transmission characteristics at the edge of shore fast sea ice. Journal of Geophysical Research: Oceans 95, 11629–11639.

Fox, C., Squire, V.A., 1994. On the oblique reflexion and transmission of ocean waves at shore fast sea ice. Philosophical Transactions of the Royal Society of London A: Mathematical, Physical and Engineering Sciences 347, 185–218.

Hassan, U.L.M., Meylan, M.H., Peter, M.A., 2009. Water-wave scattering by submerged elastic plates. The Quarterly Journal of Mechanics and Applied Mathematics 62, 321–344.

Huang, Z., Li, Y., Liu, Y., 2011. Hydraulic performance and wave loadings of perforated/slotted coastal structures: a review. Ocean Engineering 38, 1031–1053.

Karmakar, D., Soares, C.G., 2012. Oblique scattering of gravity waves by moored floating membrane with changes in bottom topography. Ocean Engineering 54, 87–100.

Kashiwagi, M., Ten, I., Yasunaga, M., 2006. Hydrodynamics of a body floating in a two-layer fluid of finite depth. part 2. diffraction problem and wave-induced motions. Journal of Marine Science and Technology 11, 150–164.

Koley, S., Sarkar, A., Sahoo, T., 2015. Interaction of gravity waves with bottom-standing submerged structures having perforated outer-layer placed on a sloping bed. Applied Ocean Research 52, 245–260.

Lin, Q., Lu, D.Q., 2013. Hydroelastic interaction between obliquely incident waves and a semi-infinite elastic plate on a two-layer fluid. Applied Ocean Research 43, 71–79.

Linton, C.M., McIver, M., 1995. The interaction of waves with horizontal cylinders in two-layer fluids. Journal of Fluid Mechanics 304, 213–229.

Liu, Y., Li, H.J., 2013. Wave reflection and transmission by porous breakwaters: A new analytical solution. Coastal Engineering 78, 46–52.

Losada, I.J., Silva, R., Losada, M.A., 1996. 3-D non-breaking regular wave interaction with submerged breakwaters. Coastal Engineering 28, 229–248.

Maiti, P., Mandal, B.N., 2014. Water wave scattering by an elastic plate floating in an ocean with a porous bed. Applied Ocean Research 47, 73–84.

Martha, S.C., Bora, S.N., Chakrabarti, A., 2007. Oblique water-wave scattering by small undulation on a porous sea-bed. Applied Ocean Research 29, 86–90.

Meylan, M.H., Squire, V.A., 1996. Response of a circular ice floe to ocean waves. Journal of Geophysical Research-All Series 101, 8869–8884.

Mohanty, S.K., Mondal, R., Sahoo, T., 2014. Time dependent flexural gravity waves in the presence of current. Journal of Fluids and Structures 45, 28–49.

Mohapatra, S.C., Ghoshal, R., Sahoo, T., 2013. Effect of compression on wave diffraction by a floating elastic plate. Journal of Fluids and Structures 36, 124–135.

Papathanasiou, T.K., Karperaki, A., Theotokoglou, E.E., Belibassakis, K.A., 2015. A higher order FEM for time-domain hydroelastic analysis of large floating bodies in an inhomogeneous shallow water environment, in: Proceedings of the Royal Society of London A: Mathematical, Physical and Engineering Sciences, The Royal Society. p. 20140643.

Sahoo, T., Yip, T.L., Chwang, A.T., 2001. Scattering of surface waves by a semi-infinite floating elastic plate. Physics of Fluids 13, 3215–3222.

Sherief, H.H., Faltas, M.S., Saad, E.I., 2004. Axisymmetric gravity waves in two-layered fluids with the upper fluid having a free surface. Wave Motion 40, 143–161.

Sollitt, C.K., Cross, R.H., 1972. Wave transmission through permeable breakwaters. Coastal Engineering Proceedings 1.

Sturova, I.V., 1999. Oblique incidence of surface waves on an elastic plate. Journal of applied mechanics and technical physics 40, 604–610.

Sturova, I.V., 2009. Time-dependent response of a heterogeneous elastic plate floating on shallow water of variable depth. Journal of Fluid Mechanics 637, 305–325.

Teng, B., Cheng, L., Liu, S.X., Li, F.J., 2001. Modified eigenfunction expansion methods for interaction of water waves with a semi-infinite elastic plate. Applied Ocean Research 23, 357–368.

Williams, T.D., Meylan, M.H., 2012. The Wiener–Hopf and residue calculus solutions for a submerged semi-infinite elastic plate. Journal of Engineering Mathematics 75, 81–106.

Xu, F., Lu, D.Q., 2010. Wave scattering by a thin elastic plate floating on a two-layer fluid. International Journal of Engineering Science 48, 809–819.

Yu, X., Chwang, A.T., 1994. Wave induced oscillation in harbor with porous breakwaters. Journal of Waterway, Port, Coastal, and Ocean Engineering 120, 125–144.